Paper 3

Farzadi, P. & Hesthammer, J. (Submitted 2006). Diagnosis of the Upper Cretaceous paleokarst and turbidite systems from the Iranian Persian Gulf using volume-based multiple seismic attribute analysis and pattern recognition. N.B.: Originally accepted for publication in the AAPG Bulletin, later rejected because the US government prohibits the publication of papers using Iranian government datasets. The manuscript has been re-submitted to Petroleum Geoscience.

Diagnosis of the Upper Cretaceous paleokarst and turbidite systems from the Iranian Persian Gulf using volume-based multiple seismic attribute analysis and pattern recognition

Pourdad Farzadi[1], Jonny Hesthammer[2]

1-Department of earth science, University of Bergen, Allegt. 41, N-5007, Bergen, Norway, E-mail: pourdad.farzadi@geo.uib.no

2- Department of earth science, University of Bergen, Allegt. 41, N-5007, Bergen, Norway, E-mail: jonny.hesthammer@geo.uib.no

Abstract

Primary depositional facies variability linked to secondary overprint of Turonian paleokarst controls the reservoir quality of the Cenomanian Mishrif reservoir, the main oil producer in southeastern Persian Gulf. Subsequent drowning of the prominent area and successive deepening of the basin during Coniacian and Santonian favored the deposition of pelagic marls of the Coniacian Laffan Formation and the development of a carbonate turbidite system within the overlying Santonian Ilam Formation. The latter occurs within slope and pelagic carbonates and consists of oil-bearing channel-reworked limestone facies. Although high-quality 3D seismic data exist over the studied oil field, it is a real challenge to map the paleokarst and turbidite deposits in 3D space using conventional seismic interpretation procedures.

This work describes a procedure using Paradigm's Seisfacies software for seismic facies classification and uses this to develop a volume-based interpretation of paleokarst geobodies and sedimentary patterns of the carbonate turbidite. A hierarchical facies classification technique combined with principal component analysis (PCA) is used to analyze a set of seismic attribute volumes that capture the seismic stratigraphic patterns inherent in the data. PCA as a data reduction algorithm greatly optimized the analysis of the attribute volumes while preserving the essential features of seismic character. A hierarchical facies classifier recognized enough variability within the seismic data to reveal details of the underlying geological features. This classification method uses multiple 3D volume attributes as input and generates a single 3D seismic facies volume (a synthesis of different attributes). Using this method, interpretive work can focus directly on geologic features in 3D space. This study gives new insights into the internal variability of paleokarst and carbonate turbidite systems in Sirri C/D oil fields (SE Persian Gulf) that are essential to estimation of reservoir volume, connectivity and variability.

Key words: Mishrif Formation; Ilam Formation; Carbonate Turbidite; Karst; PCA; Cluster Analysis

Introduction

In recent years many aspects of the structural interpretation of seismic data have become automated and more rapid (Brown 1999, 2005; Coléou *et al.* 2003; Linari *et al.* 2003; Marsh *et al*. 2005). The traditional line-by-line interpretation technique has been enhanced/replaced by techniques that operate throughout a seismic volume (e.g. Masaferro *et al.* 2003) eliminating the need for time-consuming manual horizon picking (Carillat *et al.* 2005). Although the use of automated horizon interpretation while moving through a seismic volume is valuable, it can only provide insights into the variability at the top and base of intervals and not within them. A horizon-based interpretation approach cannot provide the interpreter with a truly 3D interpretation of complex geological features (Farzadi 2006_b). In addition, caution should be used if attempting to use a single seismic attribute for the interpretation. Single seismic attribute includes features of diverse origin and the interpreter can rarely create a unique map of complex geological features in 3D space.

To move away from a purely line-based, single seismic attribute data analysis approach to one that incorporates and uses the entire data volume, requires integration of multiple seismic attribute volumes. The interpreter of multiattribute volumes faces a two-fold challenge. The first is to find the true dimensionality of a huge number of data samples (Mari *et al.* 1999) and their 3D organization in order to eliminate noise and redundant data (Farzadi 2005, 2006_b). The second challenge is to classify multiattribute seismic facies in order to recognize their meaningful 3D patterns and provide a truly 3D interpretation.

Here we employ a method for 3D multiattribute data analysis with a hierarchical classification of multivariate data in combination with a data reduction technique, namely "principal component analysis" (PCA) (Gurney 1997; Coléou *et al.* 2003; Linari *et al.* 2003).

This paper discusses a volume-based interpretation of the Turonian karsts (Harris *et al.* 1984; Alsharhan & Kendal 1991; Pasco *et al.* 1995; Philip *et al.* 1995; Montenat *et al.* 2000; Immenhauser *et al.* 2000; Farzadi 2006_a) and the development of a carbonate turbidite system (Farzadi 2005) within the Santonian Ilam Formation (James & Wynd 1965, Wood & East 1992, Motiei 1993, 1995) in the southeast Iranian Persian Gulf (Fig. 1). Age equivalent turbidites have been observed in onshore Iran (I. Sharp, personal communication), the Jabal Madar area in Oman (Montenat *et al.* 2000) and the upper Cretaceous carbonates of the Alps (Sagri 1979). The focus is on internal facies variability not recognizable using a single seismic attribute volume in study area. An emphasis is placed on ways in

which multiple attribute volume analysis in combination with PCA can greatly improve the accuracy and understanding of the geologic model.

The full interpretation process discussed here involves integration of multiattribute volumes, data reduction, facies classification (built-in Paradigm's Seisfacies software), well calibration, and, finally, building of an accurate geology model.

The advantages of this approach are: 1) It is independent of previous interpretations of particular horizons; therefore, any horizon above the target interval may be used as a reference. 2) Any combination of seismic cubes is simultaneously analyzed without limitation of the number of cubes involved in the process. 3) The least important components of the huge dataset (noise and redundant data) are removed prior to facies classification. 4) The results of data reduction and classification are reproducible. 5) The result is a single volume in 3D space that enables the interpreter to analyze the true shapes and relationships of geological patterns. The generated classification volume is shown here to be more advantageous if either "proportional slicing" (Posamentier *et al.* 1996) or "stratal slicing" (Zeng *et al.* 1998$_{a, b}$; Zeng & Hentz 2004, Farzadi 2005, 2006$_{b}$) that better follow depositional surfaces is applied for sequential seismic facies displays.

The analysis of the true shapes and relationships of geological patterns of interest is essential to prospect evaluation and reservoir characterization.

Geological Setting

The evolution of the Persian Gulf depositional basin has been a long and complex process since the Late Permian initiation of Neo-Tethys I and the Jurassic Neo-Tethys II (Smith *et al.* 1994; Glennie 1995, 2000; Sharland *et al.* 2001; Bordenave & Hegre 2005). During the Jurassic and Cretaceous, the Arabian platform in equatorial position was attached to the northern margin of Africa (Smith *et al.* 1994). In this tropical zone, a mixture of clastics, carbonates, and evaporites were deposited both laterally and iteratively through time on a low-relief shelf. Some time between the Turonian and the Campanian, obduction of oceanic crust began along the modern eastern margin of the Arabian platform (Glennie 1995). The present study focuses on the depositional features laid down during this time period (Turonian –Campanian) in Sirri C/D oil fields in the southeastern Persian Gulf (Fig. 1).

From the Permian to approximately the middle Cretaceous, the northern part of the UAE, including the study area (Fig. 1), was a tectonically passive carbonate shelf (Koop 1977; Koop & Stonely 1982; Glenni 1995, 2000; Alsharhan & Scott 2000). Throughout the Late Turonian there was a major

compressional tectonic event and the onset of folding of the Oman Mountains in the UAE. This compression continued until the central Iranian plate and the Arabian Peninsula collided in the Maastrichtian. Ocean-floor sediments emplaced rapidly onto the eastern edge of the Arabian craton as a result of this collision.

The Late Cretaceous represents a period of major change in the area of the modern Persian Gulf. The strongly progradational Cenomanian Mishrif Formation (Sarvak in Zagros) (Burchette 1993; James & Wynd 1965) – a major oil producer in the study area (Farzadi 2006_a) and elsewhere in the Persian Gulf – is formed by rudist reef development (Fig. 2). The Late Cenomanian to early Turonian was a period of generally favorable conditions worldwide for high organic productivity (Van Buchem *et al.* 2002_a). The generally rising second-order relative sea level, which allowed thick rudist reefs and skeletal banks to develop across the Arabian plate, was halted by the Turonian relative sea level fall (Loutfi *et al.* 1987; Burchette 1993; Pasco *et al.* 1995; Van Buchem *et al.* 1996, 2000, 2002_a). The effects of meteoric water dissolution and karstification were most intense beneath this regionally erosional surface (Montenat *et al.* 2000). Best reservoir quality is commonly developed within the karst-affected strata (Hunt *et al.* 2003); accurate mapping of these dissolution features (this study) is of great importance.

The Turonian unconformity was drowned beneath deep-water marls during a flooding equivalent to MFS-K150 of Sharland et al. (2001) (Fig. 2). The Laffan marls (Coniacian) corresponding to this flooding sit directly above the Turonian unconformity. Convergence along the margin of the Oman changed character from subduction to obduction during this time (Glennie 2000). On the southeastern plate margin, ophiolite emplacement occurred in the area of the Oman Mountains, and this compression probably initiated the Infracambrian salt diapirism. In response to thrusting of the Oman nappes (Robertson 1987; Burchette 1993) the erosional surface sank and was incorporated into the foreland basin which was the seat of pelagic deposits and marly turbidites. Plate flexure and subsidence enhanced by eustasy continued and the Laffan marls passed up into the argillaceous neritic/pelagic limestones of the Santonian Ilam Formation (Fig. 2). A turbidite system developed within these deep marine carbonates is discussed in the present study. A flooding event corresponding to MFS-K160 of Sharland et al. (2001) occurred near the base of the Ilam Formation (Fig. 2).

The genetic stratigraphic sequence between the two mentioned flooding events (K150_K160, Figure 2) is interpreted by Sharland et al. (2001) as a 3rd order succession driven by a combination of eustasy and subsidence resulting from structural loading of the Arabian plate margin. During this sequence, accommodation space developed significantly in most of the northern plate including the study area (Farzadi 2006_a). The study area subsided and flooded during this period resulting in the establishment of

marls and basinal carbonates on rapidly sinking preceding karstified highs. Continuous deep-water sedimentation prograded into calcareous shales with the abundant planktonic foraminifera of the Gurpi Formation indicating a deep-marine environment of Campanian age (Fig. 2). Shales at the base of the Gurpi Formation probably equate to the K170-MFS of Sharland et al. (2001).

This article focuses on 3D mapping of the paleokarst features on top of the Turonian unconformity and a turbidite system within the Santonian Ilam carbonates (Fig. 2).

Spatial pattern prognosis: Needs and constraints

A heterogeneous Late Cenomanian to Campanian depositional section is anticipated given the major changes in sedimentary environments. The swelling of the Arabian platform and later collapse of the peripheral bulge (Montenat et al. 2000) favored the development of complex depositional patterns.

The Turonian karsts cut into rudist-rich limestones of the top Mishrif reservoir as revealed by core description data (Fig. 3). These limestones are fractured with extensive development of vugy porosity. The wells that encountered karsts show significantly higher oil production rates. The heterogeneous nature of karstified limestones resulting from dual controls of depositional facies variability as well as karst distribution make it critical to map these features in 3D. As a consequence of this heterogeneity and lateral thickness variations, this karstified surface is not uniquely mapped by a single seismic attribute. Even if a unique map of this surface were available, it could not provide insight to the variability of paleokarst bodies in 3D within the data volume.

Traditional horizon-based interpretation limits the study to geometric features visible on the reservoir surface and not within it. There is a large discrepancy between the fine picture of paleokarst recognized on a horizon map and its true spatial pattern.

Recognition and mapping of the internal seismic facies variability of the overlying Laffan and Ilam Formations present a great challenge (Figs. 2 & 3). Because of the low impedance contrast between rock units and a lack of obvious reflection terminations within these deep-water sediments, manual seismic stratigraphy cannot be undertaken. Without a volume-based interpretation of multiple seismic attributes meaningful 3D patterns are lost.

Data

In this study a pre-stack time migrated seismic cube of the final migration with 300 km^2 coverage is used for the analysis. The seismic data have a bin size of 12.5 x 12.5 m., resulting in 40-fold dataset at a sampling interval of 4 ms and record length of 6 seconds. The seismic data have a broad frequency bandwidth with a dominant frequency in the range of 37-42 Hz within the study interval (Turonian-Santonian). The zone of interest is located at a relatively shallow depth (2260-2360m. / 1475-1550 ms TWT).

Wireline logs of 5 vertical wells and limited core description reports from the 2 wells were used for the interpretation.

Seismic stratigraphy and limitations

Seismic stratigraphy is the identification and interpretation of depositional sequences using seismic data. Depositional and geomorphologic information captured in seismic data are in 3D form. In seismostratigraphy it is essential to preserve this information and the connectivity of geobodies.

In large 3D surveys, manual seismic stratigraphic and facies interpretation is a time-consuming task. Seismic stratigraphic analysis, even if undertaken on a line-by-line basis, may be difficult to translate into a 3D model. Although the automated parts of the seismic interpretation such as auto tracking and formation-based seismic attribute generation have become more rapid, there is a significant amount of information for which 3D value is missed. This is evident where horizons become difficult to follow or geologic features between horizons difficult to map in the horizontal dimension. The heterogeneous nature of geologic features within seismic sequences may not be characterized by a single seismic attribute. In addition, the dominant frequency of seismic data controls the visibility of impedance layering. Limited frequency bandwidth of data makes the distinction of time stratigraphic versus time transgressive units within prograding systems problematic. Time stratigraphic and lithostratigraphic units within the same system may have boundaries that are neither coincident nor even necessarily parallel to one another (Zeng & Kerans 2003). This can lead to erroneous horizon-based seismic stratigraphic interpretation since a chronostratigraphic framework is important.

Small-scale variability observed in wireline logs represents variation in depositional energy associated with a high-frequency cyclicity that is difficult to map laterally. Interpretation of seismically thin, deep carbonate channeling systems or karstified carbonates within continuous seismic events is not repeatable without geomorphologic information from the horizontal dimension. Seismic polarity and

amplitude of thin layers are neither good indicators of lithology nor reliable references of lithofacies location and geometry (Zeng & Hentz 2004). This is true for the present study, where single horizon-based interpretations are unable to map out the paleokarst networks and deep-marine carbonate turbidites in 3D space.

Data reduction and 3D multiattribute volume classification (methodology)

The 3D volume seismic classification method requires multiple seismic attribute volumes as input. Several volume attributes can be generated from the original post-stack migrated seismic data by numerical calculations. The classification technique used in this study can be used on any combination of volumes and is limited only by the number of attributes available and hardware limitations (Coléou *et al.* 2003, Linari *et al.* 2003; Farzadi 2005, 2006$_b$). Since, however, attributes with different dimensions are used in the classification process (e.g., amplitude, impedance, discontinuity etc.), rescaling or standardization is required.

The aim of multiple attribute volume use is to increase the information available for facies classification. Seismic data and generated attribute volumes contain a huge number of data samples that are both highly redundant and noisy (Coléou *et al.* 2003). The current classification process focuses on the true dimensionality of seismic data and their organization. N-dimensional cross plots of seismic data exhibit components of elongated subclouds (clusters) and some branches. Noise tends to inflate and link clusters to remove their isolation. In this study the least important components of the data (mostly noise and redundant data) are removed prior to facies classification. Although noise is probably still a component, its reduction can help in better recognition of some geobodies in isolation.

A problem encountered in data reduction analysis is finding a suitable representation of multivariate data. For computational simplicity, these representations are sought as linear transformations of the seismic data. The linear transformation used in this study is the principal component analysis (PCA). The basic idea is to find the principal directions of components that explain the maximum amount of variance possible by number of linearly transformed components.

The PCA is a technique that can handle multiple variables at the same time. The method computes linear relationships and reduces the dimension space to project relationships with minimal loss of information. The main scope of the PCA is the representation of large sets of data in a new vectorial space with a smaller dimension than the original. This method is a powerful data-driven tool that describes the relationships between multiple variables and their classification as homogenous sets. The coordinates of the variables in a generated vectorial space represent their contribution to the new

components. The procedure treats all available information globally rather than by adding subsets of the data matrix together thus avoiding reproduction of the complex relationships among variables. The data matrix can be decomposed into a summation of eigenvalues and eigenvectors; this operation is called singular value decomposition (SVD). Singular values are equal to the positive square root of the eigenvalues of the covariance matrixes (Mari *et al.* 1999).

Once the covariance matrix is known, standard linear algebraic techniques will find the eigenvalues and eigenvectors. In practice, since multiple volumes are involved and the elements of the covariance matrixes are related to the value of the cross correlation between data matrixes (Mari *et al.* 1999), eigenvalues are calculated directly from a correlation matrix of the input attributes.

PCA examines the pattern space and finds the principal directions of variances in the multidimensional data by determining the distributions of eigenvectors. A data matrix is a linear transformation of N-dimensional Euclidean space. Eigenvalues represent the variance of the transformations when an optimal linear transform has been found. An eigenvector of a data matrix gives a direction in which that transformation is simply a scaling. The amount of scaling is the associated eigenvalue.

Eigenvector analysis can reveal patterns and their correlations in the distribution of events in 3D space. The first eigenvector represents the principal direction in which the variance is maximized. Once this direction or first component is found, only orthogonal directions are allowed for the next principal component. This iterative process will be continued until all principal components are found. The eigenvalues are positive and real for real matrixes ranked in decreasing order (Mari *et al.* 1999). In practice, the computed directions of the principal components correspond to the largest eigenvalues labeled in order of decreasing data variability.

In order to describe the data more effectively, the coordinate system is rotated so that the new X-axis lies along the maximum variance resulting in a distinct discrimination along the axis. The bulk of the data variance is then compressed into a few vector components. The first component contains the largest data variance proportionate to a co-ordinate rotation; the second component contains the largest part of the remaining variance, and so forth. Those components with eigenvalues close to or greater than “1” are generally selected as these are assumed to make the greatest contribution to the maximum spread (Fig. 4).

PCA identifies the main elongation directions within a multiattribute crossplot and enables a change of input space (where the principal axes are orthogonal to each other) via N-dimensional rotation

(Coléou *et al.* 2003). Data reduction is achieved by dropping the dimensions with the lowest variability. The output of this procedure is a set of new 3D volumes called PCA components (Fig. 4). The PCA components are ranked according to their contribution to data variability. The least important PCA components contain noise and redundant information and are usually removed (Linari *et al*. 2003). The selected important components are then projected onto the principal axes, having reduced volume, noise and redundancy for the classification process. The main trends of the crossplots are identified. These principal directions represent the heterogeneity of the multi-dimensional clouds (Fig. 4).

PCA is not a classification technique but is often used as a filter for data reduction prior to classification. In the classification process, the assumption is that two samples have the same facies class if they are characterized by similar values in all input seismic attribute volumes and, therefore, likely correspond to a similar geologic environment. Finally, a hierarchical classification procedure builds a model of classes or clusters of similar points and compares them to the original seismic data values of the entire cube. Each data value is then assigned the cluster to which it best correlates (Fig. 4).

Workflow

The complete multiattribute volume classification and interpretation workflow involves several steps, namely: 1) Structural interpretation of the bounding horizons of the study interval. The upper horizon is chosen as the reference for defining the interval for seismic facies classification. 2) Creation of seismic attribute cubes. 3) PCA analysis and examination of the calculated eigenvectors and values to drop the dimensions with the lowest variability. PCA identifies the main elongation directions (principal directions) within a multiattribute crossplot in which the principal axes are orthogonal to one another. 4) Projection of the main components onto primary principal axes. 5) Processing of the data to identify similar data points or clusters or classes. 6) Inspection of the processing results to adjust the number of classes by examining the crossplots to ensure adequate clustering and minimal overlap. 7) Classification of original seismic data and creating a single seismic facies volume. 8) Calibration and interpretation of the well. 9) Application of stratal slices for horizontal interpretation of geologic features.

In step 1, calibration of well synthetic traces to seismic amplitude traces revealed that a peak at approximately 1475 ms-TWT characterizes the top of the Ilam Formation (Fig. 5). The base of the Ilam Formation corresponds to a wide trough at the top of the Laffan Formation at approximately 1550 ms. These two horizons could be interpreted with confidence. There is no seismic response to the top of the Mishrif Formation, a well-developed karstified surface corresponding to Turonian regional unconformity.

Because 3D multiattribute seismic facies classification is based on a sample-to-sample approach, it is less sensitive to the interval definition than analyses dealing with the shape of the seismic traces. The top of the Ilam Formation was chosen as the reference for defining the interval for classification (Fig. 5). The interval of analysis was then extended from this reference to 80 ms below it to cover the entire Ilam and the Laffan Formations as well as the Turonian unconformity at the top of the Mishrif Formation.

In step 2, six attribute volumes (Fig. 5) were generated to expand the information content for the analysis. In step 3, PCA identified the main elongation directions (principal directions) within a multiattribute crossplot. The number of components is restricted so as to equal the number of attribute volumes (six components) (Fig. 6).

Because the input objects have been standardized, the variance of each object is 1 and the sum of the variances (eigenvalues) will equal the total number of input objects (the sum of the eigenvalues in Fig. 6 is 6). Data reduction is obtained by removing the dimensions with lowest variability (dropping the two last eigenvalues in Fig. 6), resulted in reducing the number of samples in the data. The eliminated components are assumed noise and redundant data. The table in figure 7 gives an indication of the contribution of each block (attribute) to the PCA components.

In step 4, the four remaining components, with a contribution to the dataset of 94.17% (Fig. 6), are projected onto the principal axis. The actual attribute values associated with each volume are replaced in the program memory with the projected values.

Steps 5 and 6 are necessarily iterative and several modifications to the number of classes are required before a satisfactory result is achieved. Based on the multidimensional plot, meaningful subsets of the input attributes are determined and a cluster node is assigned to each subset (Fig. 8). These crossplots, showing the facies model classes relative to the data spread are used to determine the appropriate number of classes. Appropriate distribution and a minimal overlap between the classes were achieved with 18 classes. All 6 input volumes (Fig. 5) have contributed to the definition of the PCA components (Fig. 8). It is, therefore, difficult to relate the results back to the input attributes using crossplots (Linari *et al.* 2003).

The critical issue in the classification process is the ordering of the classes. With clustering techniques, the continuity of the seismic trace shapes is not guaranteed. Therefore, continuous seismic trace changes may be represented with sudden changes of color. The changes of color will be the same regardless whether the changes in the seismic data are abrupt or continuous (Coléou, *et al.* 2003). With a

limited number of clusters, the results will be fairly stable but the resolution will be limited, whereas with an increased number of clusters the results lack continuity.

In step 7, a color-coded seismic facies classification volume is created. The classification process is based on a sample-to-sample approach. Samples with the same color represent the same geologic features and samples with different colors represent different features. The classification is a location-independent operator. Two classes may appear right next to each other in one crossplot but may actually be a distance apart when viewed on another crossplot (Fig. 8).

The well calibration and interpretation of step 8 is essential for evaluation of all aspects of the classification. Limited frequency bandwidth always renders imperfect seismic response to small-scale variability observed in wireline logs. The volume classification approach used in this study, however, generated results with higher interpretability of vertical details developed in 3D space (Fig. 9).

A critical condition for a good volume-based seismic facies interpretation is that facies relationships be extracted for a depositional surface (time stratigraphic surface). In step 9, stratal slices, proportionally distributed between two reference time surfaces in conformity with each of the surfaces, were computed throughout the seismic facies volume. These stratal slices identified a west-east trend of a submarine carbonate channeling system and associated lobate fans. In addition, a detailed map of the Turonian karstic systems was generated using this slicing technique. Detailed discussion of both systems follows.

Interpretation of a 3D classification

In the interpretive phase, most time was allocated to analysis of the internal stratigraphy and variability, as well as map patterns and their geological and or geophysical meaning. Accurate sequence and seismic facies mapping are linked with abundant seismic terminations (onlap, downlap, toplap and truncation) and seismic facies indicators (reflection configuration and external geometry) that can be related to depositional processes in a chronostratigraphic framework (Mitchum & Vail 1977). Much, however, of the study section (upper Cenomanian-Campanian) in the southeastern Persian Gulf comprises deep-marine successions. Seismic reflections in such formations are mostly parallel to divergent. Conventional seismic facies analysis on the basis of seismic reflection characteristics cannot detect the internal variability of the apparently low-energy deposits (Ilam Formation).

A paleokarst system related to the Turonian unconformity is encountered by the wells (Fig. 9) at the top of the Mishrif Formation (upper Cenomanian). There is no traceable seismic response to this surface. Therefore, the picture of surficial paleokarst and the population of a 3D volume are ambiguous.

The results of the present 3D classification process can be viewed in 2D sections, or in 3D space. The best understanding of the 3D seismic classification is achieved by well calibration and by viewing each class individually over calculated stratal slices. Extracted facies patterns are far more diagnostic and easier to correlate than the conventional wiggle traces of seismic reflection data.

Depositional cycles: Well calibration

Inspection of the gamma-ray logs of 5 wells and limited core description reports of 2 wells reveal important detail concerning the internal stratigraphy of the study interval. The information gleaned allows a more confident sequence stratigraphic interpretation of the succession based on the seismic facies stacking pattern. The seismic classification facies patterns make possible better correlation of depositional events in the horizontal dimension and understanding of the depositional systems.

At least 3 sequences can be differentiated in the study interval on the basis of coarsening / fining upward successions derived from gamma-ray logs (Fig. 9). A karst-modified rudist-rich limestone at the top of the Mishrif Formation characterizes the base of the study interval. The Cenomanian Mishrif Formation is a highly progradational carbonate system. Its progradation ended during an episode of uplift and emergence that favored the development of the regional Turonian exposure surface.

The accommodation increased again in the late Turonian and was incorporated with the deposition of the pelagic marls of the Laffan Formation (Fig. 9). The deposition of the Laffan Formation that corresponded to this major flooding event is marked by a high gamma-ray response. Relative sea-level rise accompanied by 3 different higher order fluctuations continued towards the top of the interval (Fig. 9). Each fluctuation or cycle consists of a couplet of decrease and increase in accommodation. The first cycle corresponds to the lower Ilam Formation and consists of peloidal, chalky limestone overlain by pyritic marls (Figs. 3 & 9). The second cycle within the middle part of the Ilam Formation comprises peloidal, argillaceous, pebbly limestones and siltstones with lithic components (lithic components are only reported in well E1) overlain by wackstones. The uppermost cycle represents an alternation of wackstones, packstone, mudstones and chalky limestones. The lower mud layer occurs above pebbly limestones and siltstones.

Interpretation results

Paleokarsts

A subaerial erosional surface with intense dissolution features (Figs. 3 & 9) truncates the Mishrif Formation of the study area, resulting in a hiatus of the Turonian carbonate deposits. The uplift leading to emergence was fast and abrupt (Farzadi 2006a). There was both uplift and fracturing (unpublished IOOC core description reports), both of which are particularly favorable factors for karstification. Attention focused on the mapping of this paleokarst system. There is no traceable seismic reflection associated with the top of the Mishrif Formation where the karstified limestones are developed. Therefore, the traditional approach of mapping the paleokarst limited to surficial features visible on dip maps (Hunt et al. 2003) is not an option. Furthermore, a tuning effect over the crests of the two structures where the Mishrif limestones become thin poses further challenge to the interpreter.

In this study, multiattribute seismic facies classification volume calibrated with well data was the source of information for the paleokarst prognosis. Seismic classification revealed the distribution and connectivity of paleokarst system away from the top Mishrif Formation as a discrete 3D volume (Fig. 10). Core description reports of wells F1 and C1 describe the top Mishrif Formation as characterized by intense dissolution features and vugy porosity. Figure 10 indicates that both wells penetrated sinkholes induced by karst development. A comparison between original seismic wiggle traces and seismic classification data shows that the latter is far more diagnostic (Fig. 10). The high resolution interpretation is supported by well data.

Calculating stratal slices through the seismic classification volume generates a plan view of karsts (Fig. 10). Manually picking the detected karsts inside a 3D seismic classification mass is, however, a significant challenge. Correlation errors in such picking can easily make the interpretation of discontinuous seismic events such as karsts erroneous.

In this study, stratal slicing (Zeng & Hentz 2004; Zeng et al. 1995, 1998 a, b) or proportional slicing (Posamentier et al. 1996) appeared most important among currently available approaches (time slicing, horizon slicing and stratal slicing). Stratal slices are proportionally distributed between the two confident reference time surfaces and conform with both surfaces. The tops of the Ilam and the Laffan Formations were chosen as reference horizons and the slicing continued downward through the Turonian unconformity (Fig. 11). The plan views shown in Figures 10 & 11 are comprehensive maps of sinkhole features deployment necessary for reservoir prognosis and further well planning.

Architecture of a carbonate turbidite system

Positive graded bedding (unpublished IOOC core description reports) and overall geometry of the channels within the Ilam Formation indicate a turbid current mechanism. Bidirectional progradation with low angle oblique stratigraphy of small sheets was observable through the classification volume. Seismic facies classification data provided an almost complete view of the architecture of a carbonate turbidite within the Ilam Formation. Application of stratal slicing made it possible to image the lateral extent of the turbidite channeling system in plan view. Following the phase of swelling and emergence recorded on the northeastern part of the Arabic platform, the area became buried again under the pelagic deposits of the Laffan Formation. Sea-level rise continued during the deposition of overlying mud-rich limestones of the Ilam Formation. This rise was a significant 3rd order development of accommodation space during the Coniacian / Santonian time (Sharland *et al.* 2001). Within the middle part of the Ilam Formation, two channel systems contribute material to the fan-shaped deposits. These are interpreted as a large turbidite system (Fig. 12).

The Ilam channeling systems extend west-southwest-east-northeast meandering extensively all along their lengths despite a high sea-level stand. These systems are connected to fan-shaped geometries relatively close to their terminations (Fig. 12). The fan surface is characterized by numerous sinuous morphological features representing meandering channels.

The analysis of the classification volume over stratal slices resulted in a grouping of these channels into two main successive individual northern and southern systems (Fig. 12). Both systems and their terminal lobs are detected within the seismic classification cube. The channels show a hummocky top surface and are locally destroyed or reworked. The number of channels increases in an easterly direction and further down-fan, mass-transport deposits are expected, to be smaller in size but occur more frequently. Channels are lens-shaped seismic facies bodies typically formed by the association of facies no. 4 and 5 (Fig. 9). This facies association is cored in well E1 and represents packstones and pebbly limestones with lithic components encased in pelagic mud-rich carbonates. Core description (Fig. 3) shows interbedding of pelitic/pyretic and chalky limestones within the lower 30m of the Ilam Formation in well E1. This unit is overlain by 3 meters of pyretic marls which pass up to 30m of pelitic, argillaceous and pebbly limestones and siltstones that encompass lithic components reported only from this well. The upper portion of the Ilam interval comprises an alternation of wackstones, packstones, mudstones and chalky limestones. Within the lower part of this interval, mud layers occur directly above pebbly limestones and siltstones. The test result of well E1 indicates that the interval corresponding to

seismic facies 4 and 5 (pebbly limestones) is oil bearing only in this well, but the production rate is non-commercial. In all other wells the Ilam Formation is non-reservoir.

The channel systems progressively evolve down-fan to lobate seismic facies units in an easterly direction. The seismic facies assemblage of these lobate units and their stacking patterns contrast with that of the more proximal channels in the more discontinuous and contorted nature of the terminal lobes. The facies of the lobate units to the east is similar to that of the channel facies, but the external configurations of these units are different (Fig. 12). The discontinuous and contorted facies of the lobes are grouped in larger, thicker, and more lens-shaped units. The maximum thickness of the channel facies is approximately 20 ms two-way travel time (30m), whereas the thickness of the same facies increases to about 50 ms (75m) in lobate units.

Unconnected channels are interpreted as being the result of over-cutting that formed out of the former aggrading channel, so that remainders of typical channel facies (facies 4 and 5, Fig. 9) can still be observed. The stacking pattern of the fan in the eastern part of the area is generated in response to lateral shifts of the channels. Channel avulsion created new channels that aggraded later, whereas the old channel is abandoned down the avulsion point.

Bi-directional downlaps and the stacking of channels with marginal overlap in relation to one another is the result of successive avulsions (Fig. 12). The origin of the direction of the avulsion and the reasons a channel avulses are beyond the scope of this study.

In both northern and southern channeling systems, the channel networks converge progressively upstream (westward) towards single channels running outside the classification volume (Fig. 12). This study cannot explain if these two channels are related to a different slope/basin system.

The network of channels is naturally organized as progressive intricate sedimentary features. In order to make an accurate chronological reference for these features dense well control is required. However, sequence analysis of available well data (Fig. 9) indicates that channel deposits occurred during a 4^{th} order relative sea-level fall following the Santonian K 160-MFS of Sharland *et al.* (2001) (Figs. 2, 3 & 9).

The oldest channels are those located to the northwest of both systems. Deposition then progressively migrated northeastward to occupy the entire eastern position of the classification volume. The architecture of both systems shows a progressive anticlockwise migration of channels to transfer the sedimentation to a depocenter located in the northeast, seemingly with a NW-SE orientation.

Synchronization of this turbidite system and the Oman ophiolite obduction suggests a structural control of the occurrence and changes of orientation of the general course of the channels.

The biota of the Ilam Formation is a mixture of displaced fossils from organisms living upslope and some deeper water bottom forms such as bryozoans (Fig. 3). There are layers of pelagic microorganisms occurring more frequently towards the upper part of the interval. These sediments are mostly chalk-textured mudstones. Channels within the studied carbonate turbidite interrupt the rhythmic and cyclic bedding of these sediments.

The presence of oil, tested within channel deposits in well E, indicates the importance of accurate mapping of these deposits.

Conclusion

The emphasis of this paper has been on a volume-based interpretation technique that exploits 3D seismic attribute volumes as input to a hierarchical seismic facies classification. The seismic classification result is a categorical variables output volume that reveals seismic stratigraphic 3D patterns inherent in all input seismic versions. 3D seismic data consist of a huge number of data points that includes noise and redundant data. By adding data volumes to the classification process, we expand the information content while the number of data samples increases dramatically, posing a major problem to the handling and analysis of the dataset.

Principal component analysis (PCA) found the principal directions of linearly transformed components of the dataset. The result of this analysis was based on eigenvalues contribution. Representation of the large dataset in a new vectorial space with a smaller dimension than the original adsorbed the noise and redundant data as separate components. Only the first four components (out of six), those with more than a 94% contribution to the data, were selected for the hierarchical classification. Noise probably remained a component, but its reduction resulted in recognition of some geologic features in isolation. The results came together with confidence measures for each seismic facies as calibrated with well data. This approach uses the entire data volume and frees the interpretation from the limitations of a horizon-based procedure. The resulting 3D multiattribute seismic facies classification enabled detail stratigraphic interpretation of the Turonian paleokarst and a prospect carbonate turbidite within the Ilam Formation in the southeast Iranian Persian Gulf. Sequential stratal slicing throughout the classification volume provided important new geological information and detail, reflecting the true shape, connectivity and heterogeneity of the main features of interest, as has been shown in this work for paleokarst and carbonate turbidite systems.

The study has provided the first 3D realization of the Turonian paleokarst and a Santonian turbidite system that are of significant importance for present production enhancement of the Mishrif reservoir and future exploration in the Ilam Formation.

The mapping of paleokarst as a controlling factor in the oil production rate from the Mishrif Formation and a carbonate turbidite system that explains the presence of oil in the Ilam Formation is a step towards pattern recognition for hydrocarbon exploration in the southeast Iranian Persian Gulf.

Acknowledgements

We acknowledge the support from IOOC and NIOC for providing 3D seismic and well data. We wish to thank Norsk-Hydro (Norway) for its financial support of the research project, and the University of Bergen for system support and a supportive research environment. Drs. David Hunt and Ian Sharp provided guidance throughout the work. The manuscript benefited from the comments and suggestions of Profs. William Heland-Hansen and Michael Talbot. Dr. Mojaheed-al-Hosseini (Editor-in-chief GeoArabia) gave permission for reproduction of Figure 2. Stratimagic and SeisFacies are trademarks of Paradigm Geophysical and were used for this study; provision of this software is gratefully acknowledged.

References:

Alsharhan, A.S. & Kendall, C.G.St.C. 1991. Cretaceous chronostratigraphy, unconformities and eustatic sea-level changes in the sediments of Abu Dhabi U.A.E. *Cretaceous Research,* **12**, 379–401.

Alsharhan, A.S. & Scott, R.W. 2000. Hydrocarbon potential of Mesozoic carbonate platform-basin systems, U.A.E. *In:* Alsharhan, A.S. & Scott, R.W. (eds) *Middle East models of Jurassic/Cretaceous carbonate systems.* Society of Economic Paleontologists and Mineralogists Special Publication, **69**, 335–358.

Bordenave, M.L. & Hegre, J.A. 2005. The influence of tectonics on the entrapment of oil in the Dezful Embayment, Zagros FoldBelt, Iran. *Journal of Petroleum Geology,* **28/4**, 339-368.

Brown, A.R. 1999. Interpretation of three-dimensional seismic data, 5th edn. *American association of Petroleum Geologists Memoir*, **42**, 514

Brown, A.R. 2005. Pitfalls in 3D seismic interpretation, keynote presentation at the 11th annual 3-D seismic symposium, Denver. The leading edge, July 2005, 716-717.

Burchette, T.P. 1993. Mishrif Formation (Cenomanian–Turonian), southern Arabian Gulf: Carbonate platform growth along a cratonic basin margin. *In:* Simo, J.A.T., Scott, R.W. & Masse, J.P. (eds) *Cretaceous carbonate platforms.* American Association of Petroleum Geologists Memoir, **56**, 185–199.

Carillat, A., Hunt, D., Randen, T., Sonneland, L. & Elvebakk, G. 2005 Automated mapping of carbonate build-ups and paleokarst from the Norwegian Barents Sea using 3D seismic texture attributes. In: Doré, A.G. and Vining, B.A. (proceedings) Petroleum Geology: North-West Europe and Global Perspectives, 6th Petroleum Geology Conference, Queen Elizabeth II Conference Centre, London, 6-9 October 2003. **2**, 1595-1611

Coléou T., Poupon, M. & AZBEL, K. 2003. Unsupervised seismic facies classification: A review and comparison of techniques and implementation. Interpreter's corner, The Leading Edge, October 2003, 942-953.

Farzadi, P. 2005. Stratal geometries of the Cretaceous carbonate systems- Application of multiple volume attribute analysis to 3D seismic data from the Persian Gulf. Middle East to Far East Carbonate Reservoirs: Exploration, Development and Exploitation, Petroleum Exploration Society of Great Britain, Carbonate Conference, London, 15th and 16th November 2005.

Farzadi, P. 2006_a. The development of Middle Cretaceous carbonate platforms, Persian Gulf, Iran: Constraints from seismic stratigraphy, well and biostratigraphy. *Petroleum Geoscience*, **12**, 59-68.

Farzadi, P. 2006_b. Seismic facies analysis based on 3D multi-attribute volume classification, Dariyan Formation, SE Persian Gulf. *Journal of Petroleum Geology,* **29/2**, 1-16

Glennie, K.W. 1995. The geology of the Oman Mountains: an outline of their origin. Scientific Press, Beaconsfield, UK.

Glennie, K.W. 2000. Cretaceous tectonic evolution of Arabia's eastern plate margin: A tale of two oceans. *In:* Alsharhan, A.S. & Scott, R.W. (eds) *Middle East models of Jurassic/Cretaceous carbonate systems.* Society of Economic Paleontologists and Mineralogists Special Publication, **69**, 9–20.

Gurney, K. 1997, An introduction to Neural network: London, UCL press, 234p.

Harris, P.M., Frost, S.H., Seiglie, G.A. & SCHENEIDERMANN, N. 1984. Regional unconformities and depositional cycles, Cretaceous of the Arabian Peninsula. *In:* J.S. Schlee (ed.), *Interregional unconformities and hydrocarbon accumulation*. American Association of Petroleum Geologists Memoir, **36**, 67-80.

Hunt, D., Elvebakk, G. Rafaelsen, B., Pajchel, J., Hogstad, K., Robak, H. & Randen, T. 2003, Paleokarst recognition & 3D distribution: new insights from the upper Paleozoic, Loppa High, Barent sea. *Europian Association of Geoscientists & engineers*, *65th conference & Exhibition, Stavanger, Norway, Extended Abstracts.* EAGE, Netherlands, 00-01.

Immenhauser, A., Creusen, A., Esteban, M. & Vonhof, H.B. 2000. Recognition and interpretation of polygenic discontinuity surfaces in the Middle Cretaceous Shu´aiba, Nahr Umr and Natih Formations of Northern Oman. *GeoArabia*, **5** (2), 299-322.

JAMES, G.A. & WYND, J.G. 1965. Stratigraphic Nomenclature of the Iranian Oil Consortium Agreement Area. *American Association of Petroleum geologists Bulletin*, **49**, 2182-2245.

KOOP, W. J. 1977. The paleostructural history of SW Iran and its effect on hydrocarbon generation and entrapment. Oil Service Company of Iran (OSCO), internal report number 1292.

KOOP, W. J. & STONELEY, R. 1982. Subsidence History of the Middle East Zagros Basin, Permian to recent. *In:* Kent, P., Bott, M.H.P., McKenzie & Williams, C.A., (eds), *The evolution of Sedimentary Basins, Philosophical Transactions of the Royal Society of London*, Part A, **305**, 149–168.

Linari, V., Santiago, M., Pastore, C., Azbel, K. & Poupon, M. 2003. Seismic facies analysis based on 3D multi-attribute volume classification, La Palma field, Maracaibo, Venezuela. *The Leading Edge*, January 2003, 32-36.

Loutfi, G., Baslaib, S.M. & Abu Hamd, M. 1987. Cenomanian stratigraphic traps in western Abu Dhabi, U.A.E. Paper SPE 15684, presented at the 5th Middle East Oil Show, Bahrain, Society of Petroleum Engineers, 1–8.

Mari, J.L., Glangeaud, F. & Coppens, F. 1999. *Signal processing for geologists and geophysicists.* Institut francais du pétrole, 458 PP.

Marsh, J.T., Tyrrell, J. & Evins, L. 2005. Role of automated techniques in improving volume-based structural interpretation. Europian association of Geoscientists & engineers, *First Break*, **23**, 89-93.

Masaferro, J.L., Bourne, R. & Jsuffred, J.L. 2003. 3D visualization of carbonate reservoirs. Interpreter's corner, *The Leading Edge*, January 2003, 18-25.

Mitchum, R.M. & P.R. Vail 1977. Seismic stratigraphy and global change of sea level: part 7, Seismic stratigraphic interpretation procedure, *In:* Payton, C.E. (eds) *Seismic stratigraphy*: American Association of Petroleum Geologists Memoir, **26**,135-143.

Montenat, C., Soudet, H.-J., Barrier, P. & Chereau, A. 2000. Karstification and tectonic evolution of the Jabal Madar (Adam Foothills, Arabian Platform) during the Upper Cretaceous. *Bulletin Centre Recherche Elf Exploration Production.,* **22**, 161–183.

Motiei, H. 1993. Geology of Iran: Stratigraphy of Zagros. Geological Survey of Iran (in Farsi).

Motiei, H 1995. Petroleum geology of Zagros-1. Geological Survey of Iran (in Farsi), 589pp.

Pascoe, R.P., Evans, N.P. & Harland, T.L. 1995. The generation of unconformities within the Mishrif and Laffan formations of Dubai and adjacent areas: applications to exploration and production. *In:* Husseini, M.I. (ed.) *Middle East Petroleum Geosciences, Geo'* 94*,* **2**. Gulf PetroLink, Bahrain, 749–760.

Philip, J., Bogomano, J. & Al-Maskiry, S. 1995. Cenomanian–Early Turonian carbonate platform of northern Oman: Stratigraphy and Palaeoenvironments. *Palaeogeography, Palaeoclimatology, Palaeoceology,* **119**, 77–92.

Posamentier, H.W., Dorn, G.A., Cole, M.J., Beierle, C.W. & ROSS, S.P. 1996. Imaging elements of depositional systems with 3-D seismic data: A case study: Gulf Coast Section, SEPM Foundation, 17th Annual Research Conference. 213-228.

Robertson, A.H.F. 1987. Upper Cretaceous Muti Formation- Transition of a Mesozoic carbonate platform to a foreland basin in the Oman Mountains, *Sedimentology*, **4**, 1123-1142.

Sagri, M. 1979. Upper Cretaceous carbonates of the Alps and Apennines deposited below the calcite compensation level. *Journal of Sedimentary Petrology*, **49/1**, 23-28.

Sharland, P.R., Archer, R., Casey, D.M. *et al.* 2001. *Arabian plate sequence stratigraphy.* GeoArabia Special Publication, **2**. Gulf PetroLink, Bahrain, 261–278.

Smith, A.G., Smith, D.G. & Funnell, B.M. 1994. *Atlas of Mesozoic and Cenozoic coastlines.* Cambridge University Press, Cambridge.

Van Buchem, F.S.P., Razin, P., Homewood, P.W. *et al.* 1996. High-resolution sequence stratigraphy of the Natih formation (Cenomanian/Turonian) in northern Oman: Distribution of source rocks and reservoir facies. *GeoArabia,* **1** (1), 65–91.

Van Buchem, F.S.P., Daniel, J.M., Mengus, J.M., Homewood, P. & Droste, H. 2000. The Natih carbonate petroleum system (Cenomanian/Turonian; N. Oman) – an integrated study of reservoir facies, source rocks and fracture patterns in a high resolution sequence stratigraphic framework. American Association of Petroleum Geologists, Field Seminar Guidebook.

Van Buchem, F.S.P., Razin, P., Homewood, W., Oterdoom, H. & Philip, J. 2002*a*. Stratigraphic organization of carbonate ramps and organic-rich intrashelf basins: Natih Formation (middle Cretaceous) of northern Oman. *American Association of Petroleum Geologists Bulletin,* **86**, 21–54.

Wood, J.R. & East, G.R. 1992. An integrated approach to the recognition and characterization of a fractured limestone reservoir in the Ilam Formation, Fateh Field, Dubai – U.A.E. *Society of Petroleum Engineers*, SPE24510 (ADSPE 1002).

Zeng, H., Backus, M.M., Barrow, K.T. & N. Tyler 1995, Three dimensional seismic modeling and seismic facies imaging: Gulf coast Association of geologic societies Transactions, **45**, 621-528.

Zeng, H., Backus, M.M., Barrow, K.T. & Tyler, N. 1998a. Stratal slicing: Part I, Realistic 3-D seismic model. *Geophysics*, **63** (2), 502-513.

Zeng, H., Henry, S.C. & Riola, J.P. 1998b. Stratal slicing: Part II. Real seismic data: *Geophysics*, **63/2**, 514-522.

Zeng, H. & Kerans, C. 2003. Seismic frequency control on carbonate seismic stratigraphy: A case study of the Kingdom Abo sequence, West Texas: *American Association of Petroleum Geologists Bulletin*, **87**, 2, 273-293.

Zeng, H., & Hentz, T.F. 2004. High frequency sequence stratigraphy from seismic sedimentology: Applied to Miocene, Vermilion Block 50, Tiger shoal area, offshore Louisiana. *American Association of Petroleum Geologists Bulletin*, **88** (2), 153-174.

Figure captions

Fig. 1: Location map of the study area in the SE Persian Gulf (arrow) and a time structure map of the Ilam Formation (Santonian) showing two salt-driven domal structures and the location of five vertical wells.

Fig. 2: Chronostratigraphy of the Late Cretaceous in the Middle East region (after Sharland, et al., 2001). The studied interval extends from the Turonian unconformity at the top of the Mishrif Formation through the Laffan and Ilam Formations and correlates with the lower part of the Arabian plate megasequence 9 (AP9). Deposition of the two latter corresponds to two third-order MFS (k150 and k160) and continuous deepening of the depositional basin occurred in the study area (see text for details).

Fig. 3: The study interval in well E1 (location in Figure 1). Gamma ray, porosity log and available core description information are shown. Intense dissolution at the top Mishrif Formation corresponds to the Turonian erosional surface. A high gamma ray response indicates drowning of this surface beneath deep-water Laffan marls that passed up into the argillaceous limestones of the Ilam Formation. At least three gamma ray-derived coarsening/fining sequences are observed within the studied interval. Fossils indicate a transition from neritic to pelagic dominance towards the top of the interval.

Fig. 4: Schematic diagram of PCA analysis showing a 3D crossplot of three standardized input volumes (volume 1- volume 3) reduced to two PCA components (PCA1 and PCA2) after eliminating the components with less contribution to maximum elongation trends. Rotation of the coordinate system for each component gives distinct discrimination of the data cloud along one of the axes leading to recognition of meaningful patterns. The PCA components are used to generate a single seismic volume through a hierarchical classification of the original seismic data. Each value from the original data is assigned to the cluster to which it best correlates. The clusters are sorted in a progressive sequence until a single classification data volume is generated.

Fig. 5: Six seismic attribute volumes extracted from final migrated 3D seismic data through numerical calculations. An arbitrary line connecting wells E1 and D1 (location in Figure 1) is shown throughout each attribute volume. The generated seismic volume versions are used as input into PCA analysis to expand the information content within the studied interval (80 ms). The thickness is two-way travel time in milliseconds.

Fig. 6: Crossplot showing the calculated eigenvalues for the six components. The components with values close to or greater than 1, contribute significantly to the main elongation trend of the dataset. The

remaining components are usually either redundant data or noise and are eliminated from pattern analysis. The table(inset) shows that the contribution of first four components to the dataset is 94.17%.

Fig. 7: Components variable correlation showing the contribution of each input attribute (see figure 5) to the generated PCA components. The weight of each component on the six input variables is shown in the table.

Fig. 8: Two-dimensional cross-plot of data distribution plotted against different principal axes. Note that two adjacent classes in one crossplot may be a distance apart on another crossplot.

Fig. 9: Seismic classification data at well locations. Coarsening/fining upward depositional sequences derived from gamma ray log are shown for each well. The gamma ray-derived high frequency cyclicity is superimposed on a general 3rd –order increase in accommodation space shown in Figure 2. Seismic facies are numbered sequentially. Oil production rate from the Mishrif Formation in well C1 (facies class 9) is significantly higher than other wells. Well E1 is the only well showing oil, although it is non-commercial, within the middle Ilam Formation (facies class 5)

Fig. 10: The distribution of paleokarst system on the Turonian erosional surface is illustrated in plan view (a and b). Wells F1 and C1 penetrate two dissolution-related depressions in the rudist-rich limestones of the top Mishrif Formation. Well C1 has a significantly higher rate of production. Classification data made it possible to map each of these features in isolation, showing that Well C1 penetrates the middle of a karst collapse breccia. Original seismic wiggle traces (c and d) are compared with classification data at well locations.

Fig. 11: Two random lines through both original stacked amplitude data volume and classification volume (a) are shown (b and c). The position of the proportional slice (a) is shown over the random line (PS in b). The karstified surface (Ka in (c) can be interpreted with far more detail using classification data (c).

Fig. 12: The channeling systems of a carbonate turbidite within the middle part of the Santonian Ilam Formation in plan view (a). Three random lines through the classification volume (b, c and d) show the geometry of the different parts of this system (location of the random lines are shown by dashed lines in a). The position of the proportional slice is shown over the random lines (dotted lines in b, c and d). Well E1 penetrates and demonstrates oil shows from one of the abandoned channels.

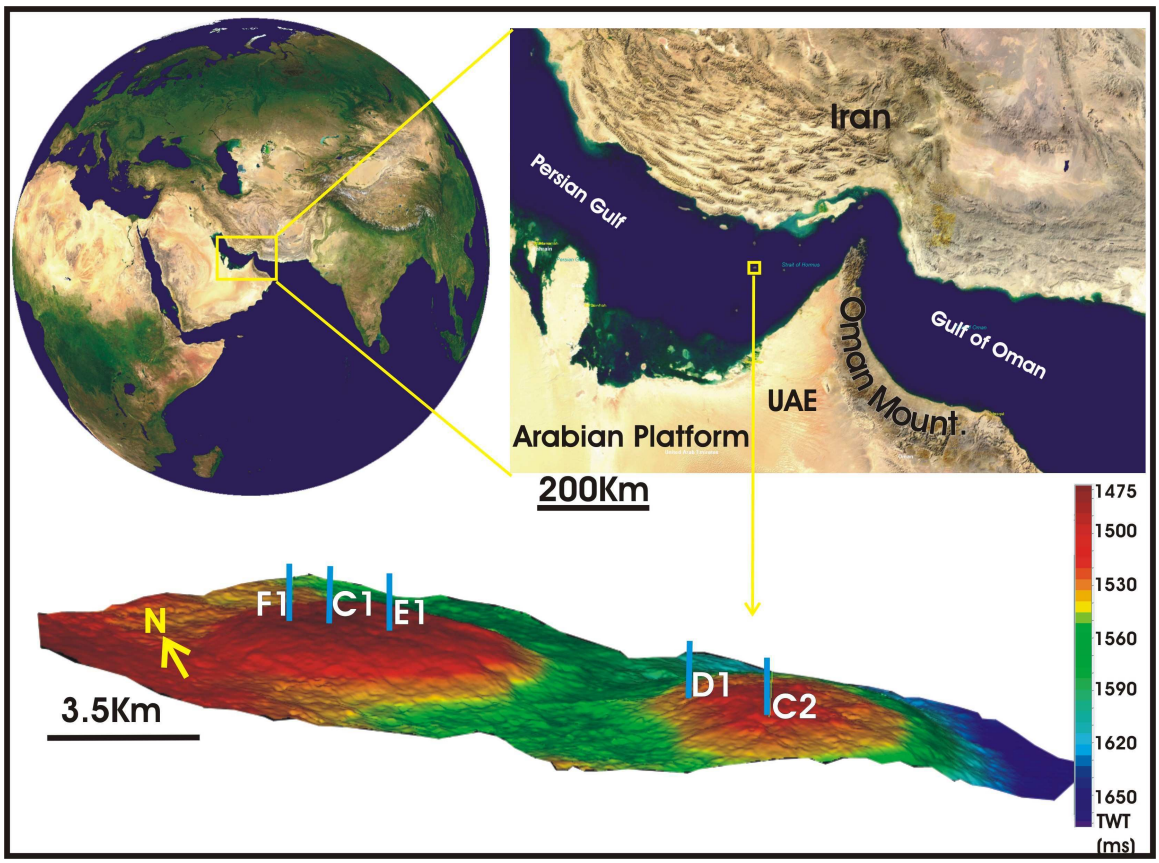
Iran
Persian Gulf
Gulf of Oman
Oman Mount.
UAE
Arabian Platform
200Km
N
F1
C1
E1
D1
C2
3.5Km
1475
1500
1530
1560
1590
1620
1650
TWT
(ms)

Figure 1

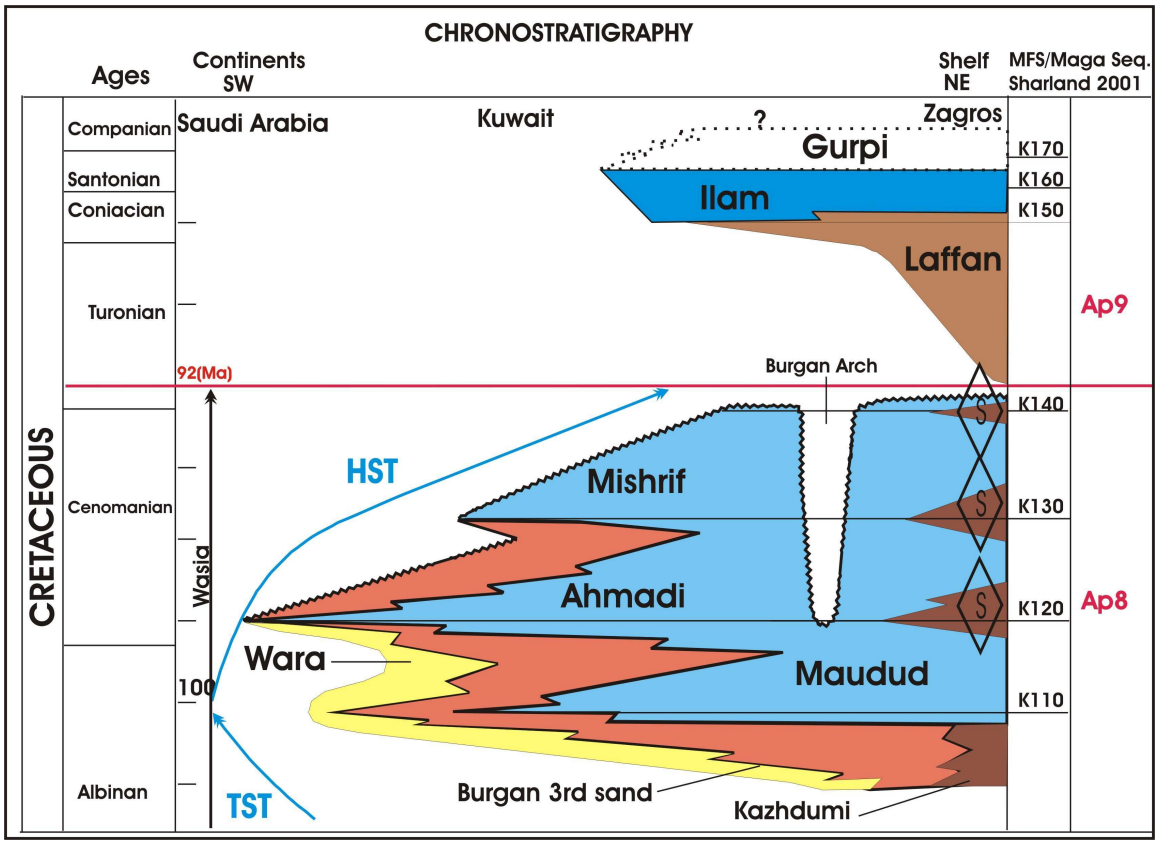
CHRONOSTRATIGRAPHY
Ages
Continents
SW
Shelf
NE
MFS/Maga Seq.
Sharland 2001
CRETACEOUS
Companian
Santonian
Coniacian
Turonian
Cenomanian
Albinan
Saudi Arabia
Kuwait
?
Zagros
Gurpi
Ilam
Laffan
Ap9
92(Ma)
Burgan Arch
K170
K160
K150
K140
K130
K120
K110
Ap8
HST
Mishrif
Ahmadi
Wara
Maudud
Wasia
100
TST
Burgan 3rd sand
Kazhdumi

Figure 2

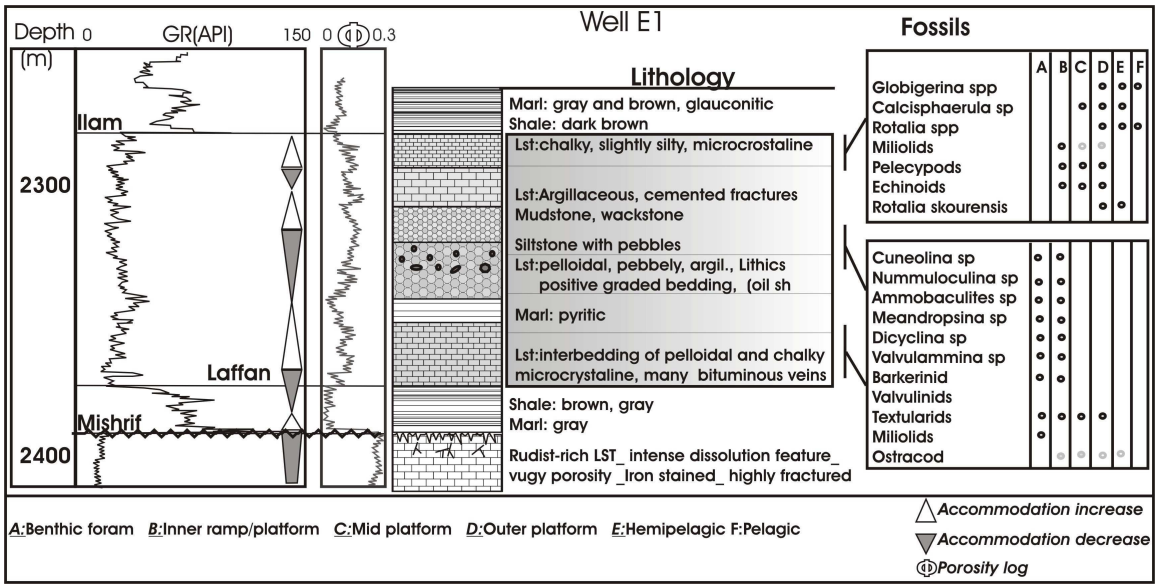
Depth
(m)
0
GR(API)
150
0
0.3
Well E1
Lithology
Fossils
Ilam
2300
Laffan
Mishrif
2400
Marl: gray and brown, glauconitic
Shale: dark brown
Lst:chalky, slightly silty, microcrostaline
Lst:Argillaceous, cemented fractures
Mudstone, wackstone
Siltstone with pebbles
Lst:pelloidal, pebbely, argil., Lithics
positive graded bedding, (oil sh
Marl: pyritic
Lst:interbedding of pelloidal and chalky
microcrystaline, many bituminous veins
Shale: brown, gray
Marl: gray
Rudist-rich LST_ intense dissolution feature_
vugy porosity _Iron stained_ highly fractured
A
B
C
D
E
F
Globigerina spp
Calcisphaerula sp
Rotalia spp
Miliolids
Pelecypods
Echinoids
Rotalia skourensis
Cuneolina sp
Nummuloculina sp
Ammobaculites sp
Meandropsina sp
Dicyclina sp
Valvulammina sp
Barkerinid
Valvulinids
Textularids
Miliolids
Ostracod
A:Benthic foram B:Inner ramp/platform C:Mid platform D:Outer platform E:Hemipelagic F:Pelagic
Accommodation increase
Accommodation decrease
Porosity log

Figure 3

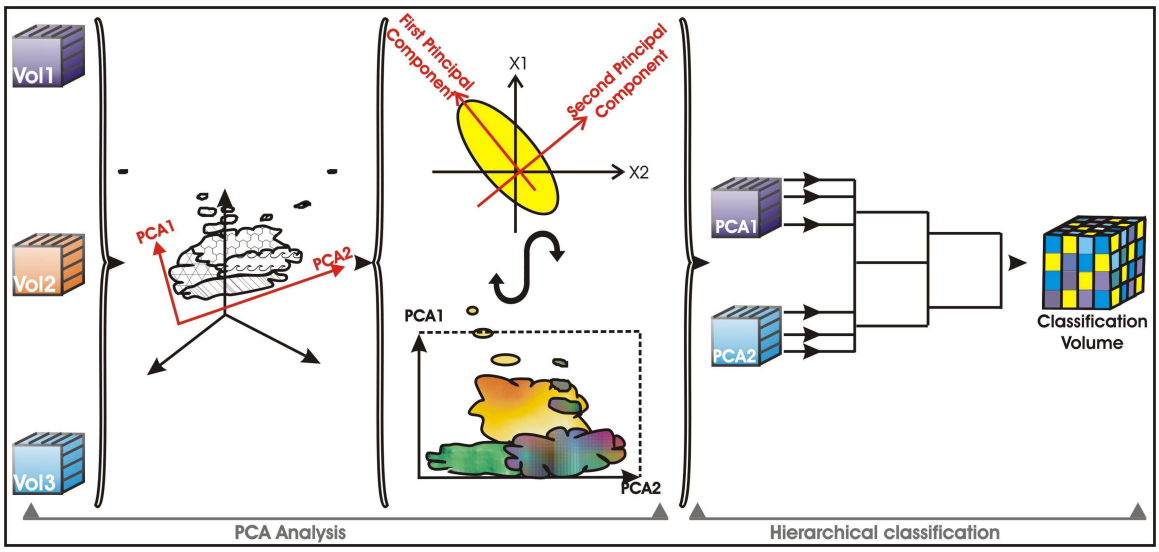
Vol1
Vol2
Vol3
PCA1
PCA2
First Principal Component
Second Principal Component
X1
X2
PCA1
PCA2
PCA1
PCA2
Classification Volume
PCA Analysis
Hierarchical classification

Figure 4

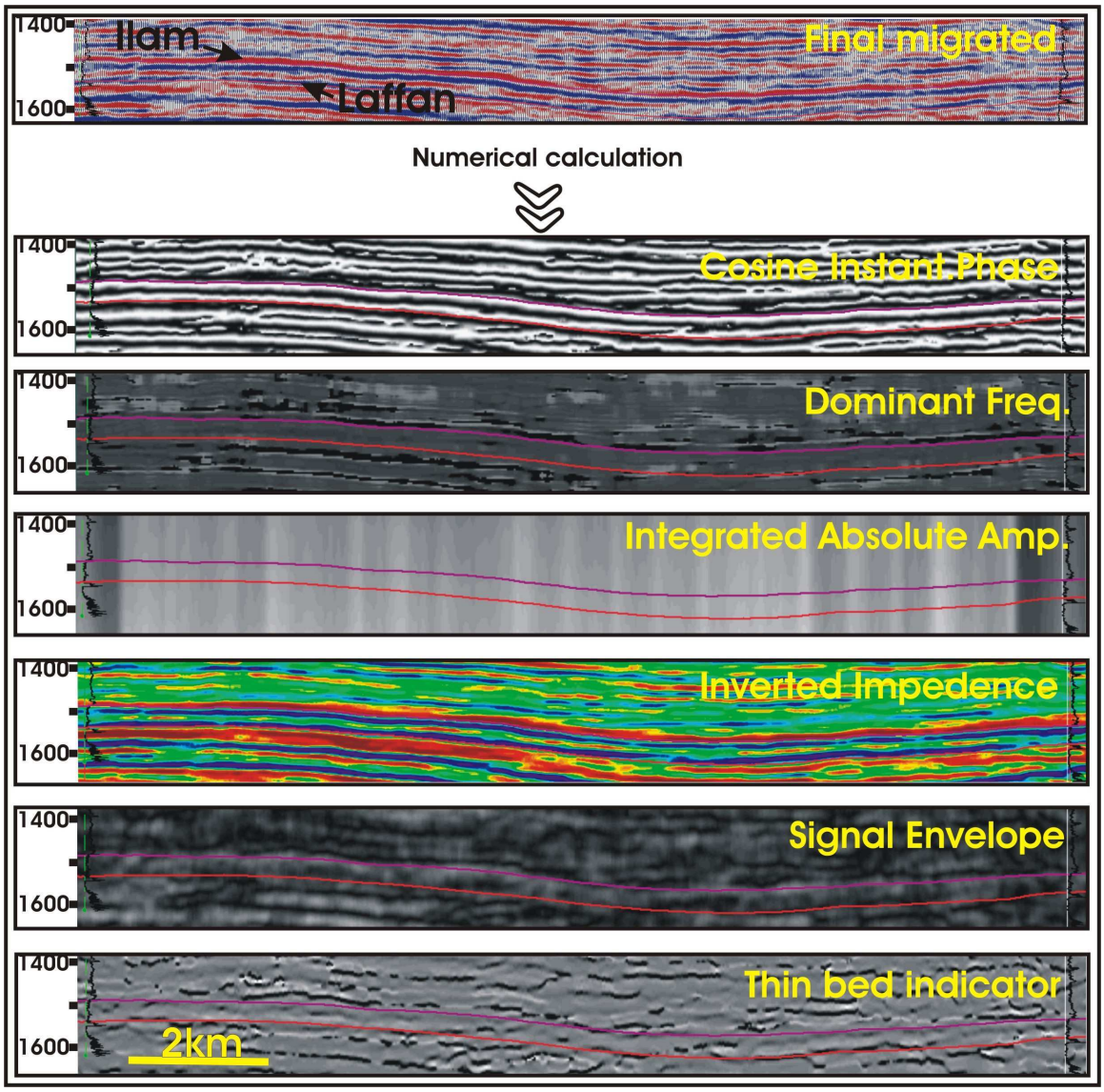
1400
1600
Ilam
Laffan
Final migrated
Numerical calculation
Cosine Instant.Phase
Dominant Freq.
Integrated Absolute Amp.
Inverted Impedence
Signal Envelope
Thin bed indicator
2km

Figure 5

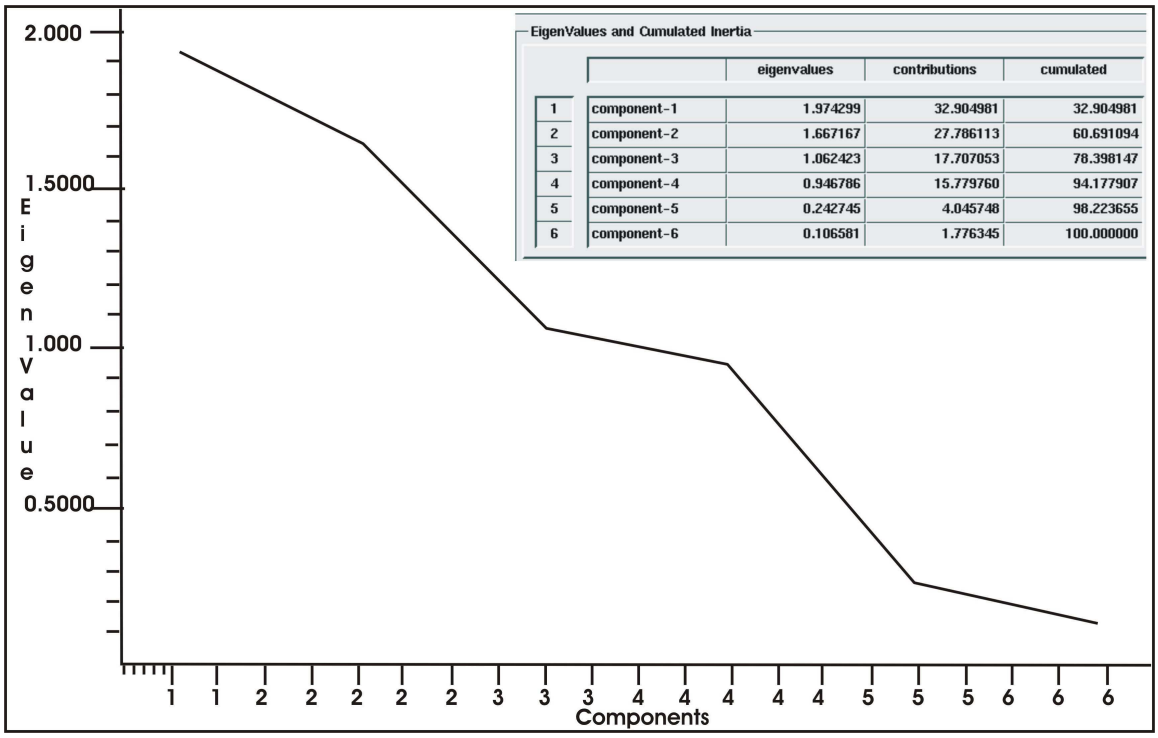
EigenValues and Cumulated Inertia
eigenvalues
contributions
cumulated
1 component-1 1.974299 32.904981 32.904981
2 component-2 1.667167 27.786113 60.691094
3 component-3 1.062423 17.707053 78.398147
4 component-4 0.946786 15.779760 94.177907
5 component-5 0.242745 4.045748 98.223655
6 component-6 0.106581 1.776345 100.000000
2.000
1.5000
1.000
0.5000
Eigen Value
1 1 2 2 2 2 2 3 3 3 4 4 4 4 4 5 5 5 6 6 6
Components

Figure 6

Components-variables correlations		Thin.bed.indic.	Signal-envelop	Invert.imped.	Int.abs.amp.	Dom.freq.	Cos.inst.phase
1	component-1	-0.194451	0.927703	0.231054	0.962482	0.928257	0.041098
2	component-2	0.100834	-0.040098	0.909805	-0.103345	-0.099700	0.939386
3	component-3	-0.974236	-0.182918	0.061202	-0.010554	-0.027045	0.033461
4	component-4	0.018154	-0.174313	-0.291303	0.004526	0.232637	0.297929
5	component-5	0.041449	-0.226445	0.173610	-0.051053	0.251849	-0.161145
6	component-6	-0.028947	0.150458	-0.011181	-0.245377	0.100597	0.004040

Figure 7

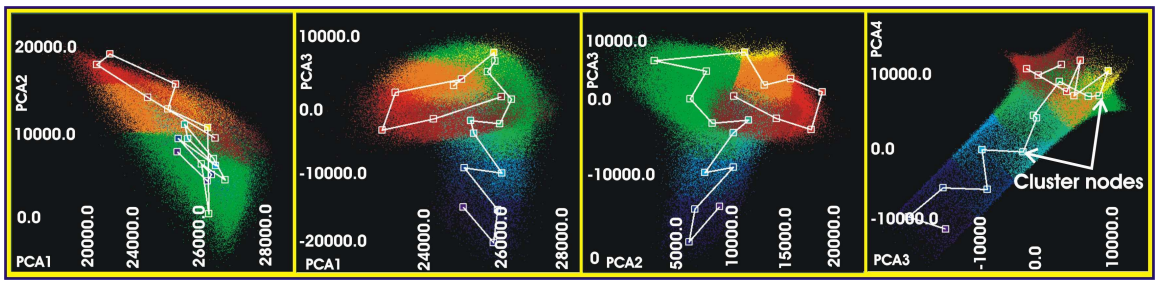
20000.0
PCA2
10000.0
0.0
PCA1
20000.0
24000.0
26000.0
28000.0
10000.0
PCA3
0.0
-10000.0
-20000.0
PCA1
24000.0
26000.0
28000.0
10000.0
PCA3
0.0
-10000.0
0 PCA2
5000.0
10000.0
15000.0
20000.0
PCA4
10000.0
0.0
-10000.0
PCA3
-10000
0.0
10000.0
Cluster nodes

Figure 8

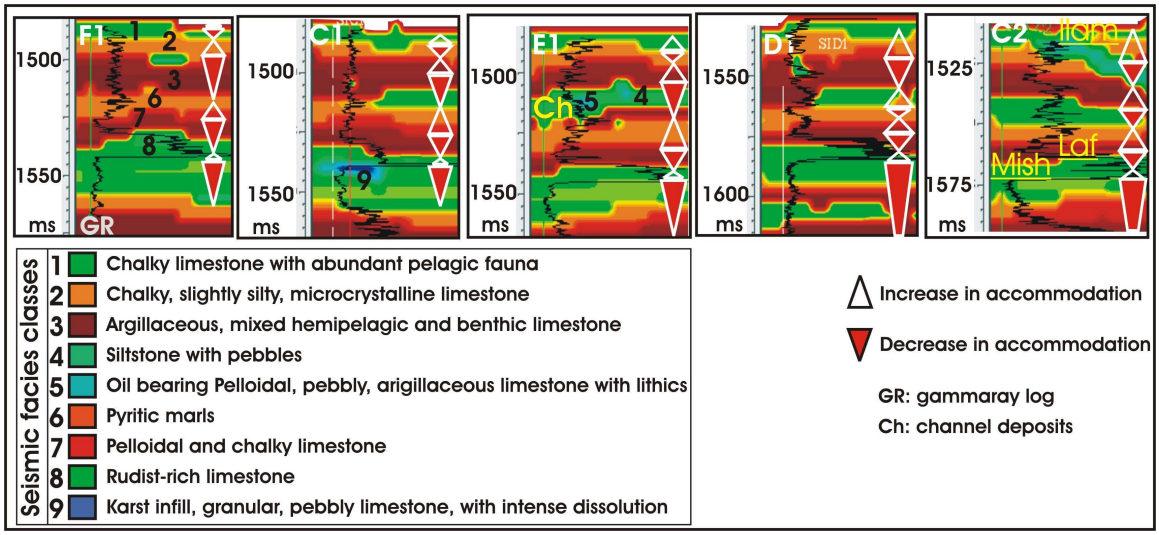
F1
CT
E1
D
C2
1500
1550
1600
1525
1575
ms
GR
Ch
SIDI
Mish
Laf
Seismic facies classes
1 Chalky limestone with abundant pelagic fauna
2 Chalky, slightly silty, microcrystalline limestone
3 Argillaceous, mixed hemipelagic and benthic limestone
4 Siltstone with pebbles
5 Oil bearing Pelloidal, pebbly, arigillaceous limestone with lithics
6 Pyritic marls
7 Pelloidal and chalky limestone
8 Rudist-rich limestone
9 Karst infill, granular, pebbly limestone, with intense dissolution
Increase in accommodation
Decrease in accommodation
GR: gammaray log
Ch: channel deposits

Figure 9

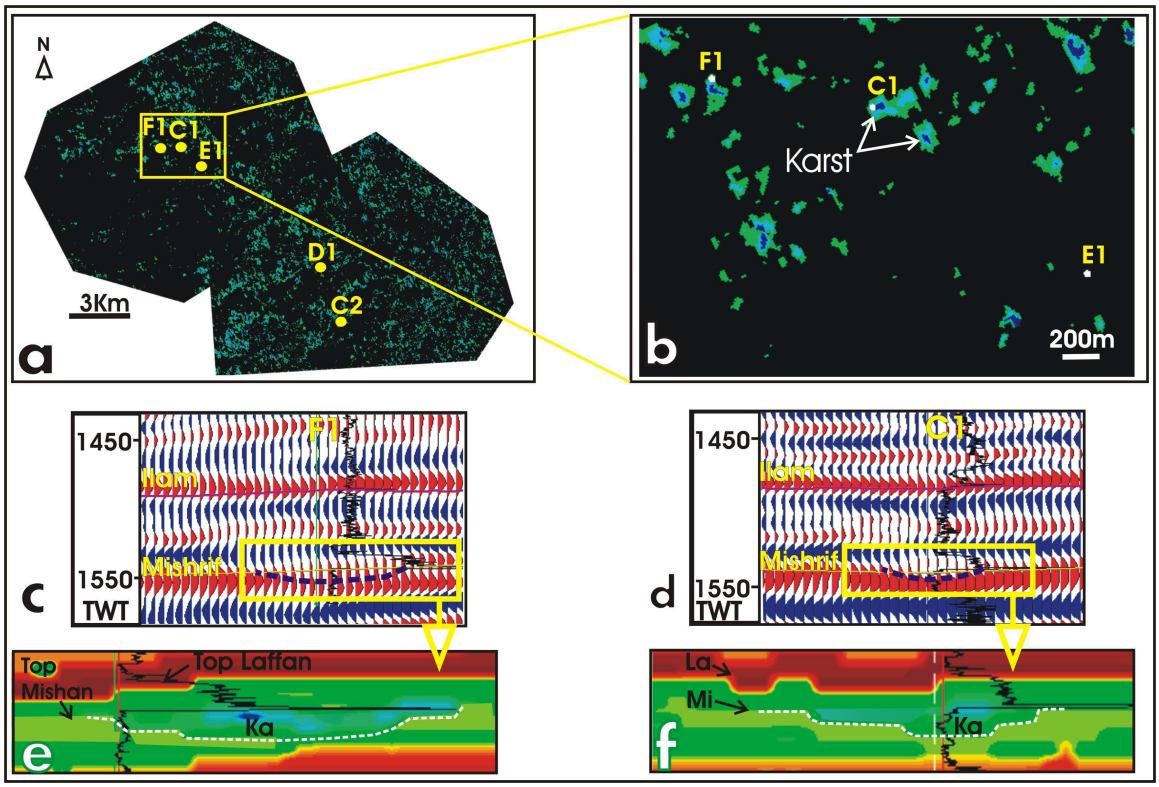
N
F1
C1
E1
D1
C2
3Km
a
F1
C1
Karst
E1
200m
b
1450
1550
TWT
Ilam
Mishrif
F1
c
C1
d
Top
Mishan
Top Laffan
Ka
e
La
Mi
Ka
f

Figure 10

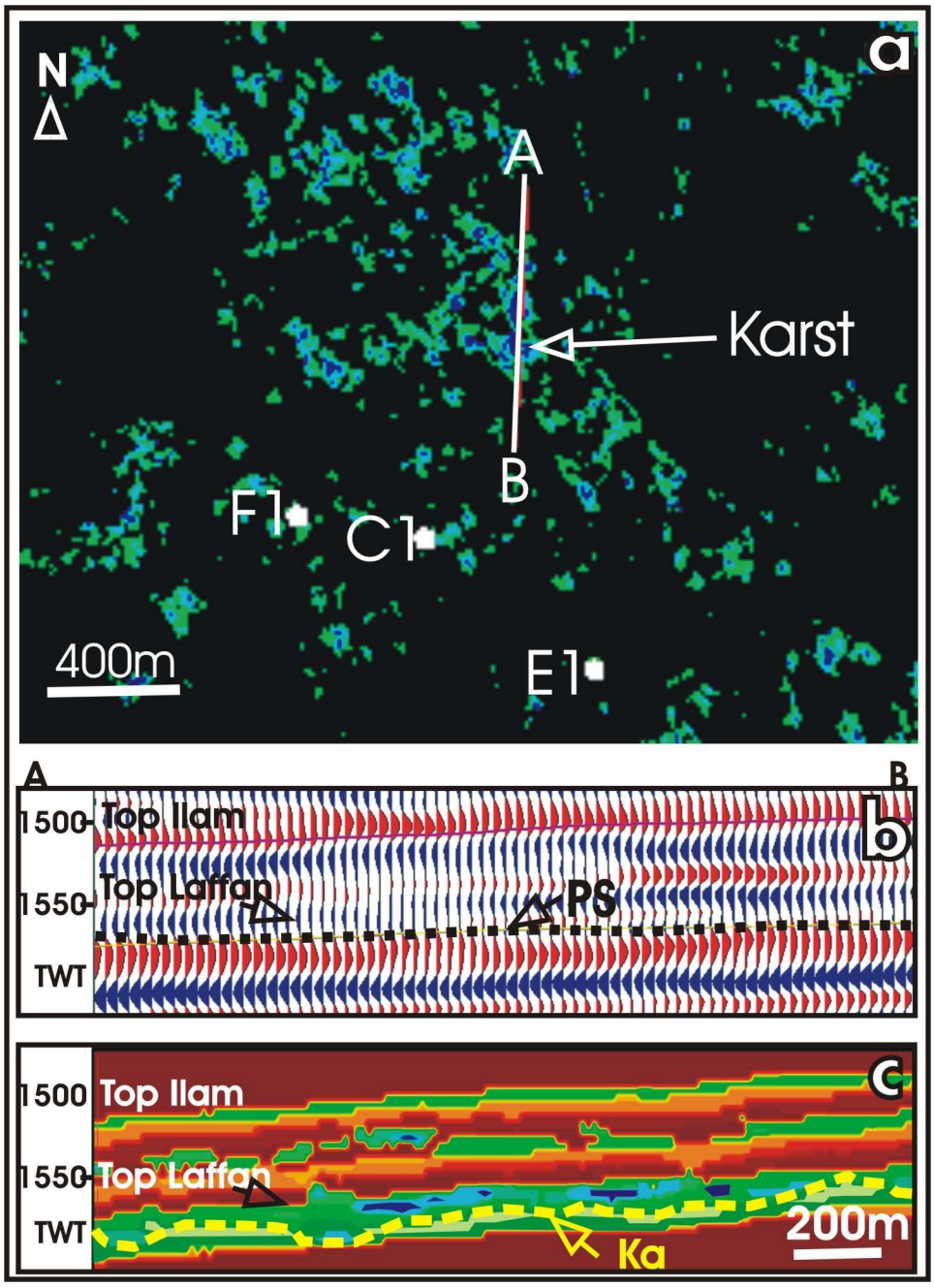
N
a
A
B
Karst
F1
C1
E1
400m
A
B
1500
Top Ilam
b
1550
Top Laffan
PS
TWT
1500
Top Ilam
c
1550
Top Laffan
TWT
Ka
200m

Figure 11

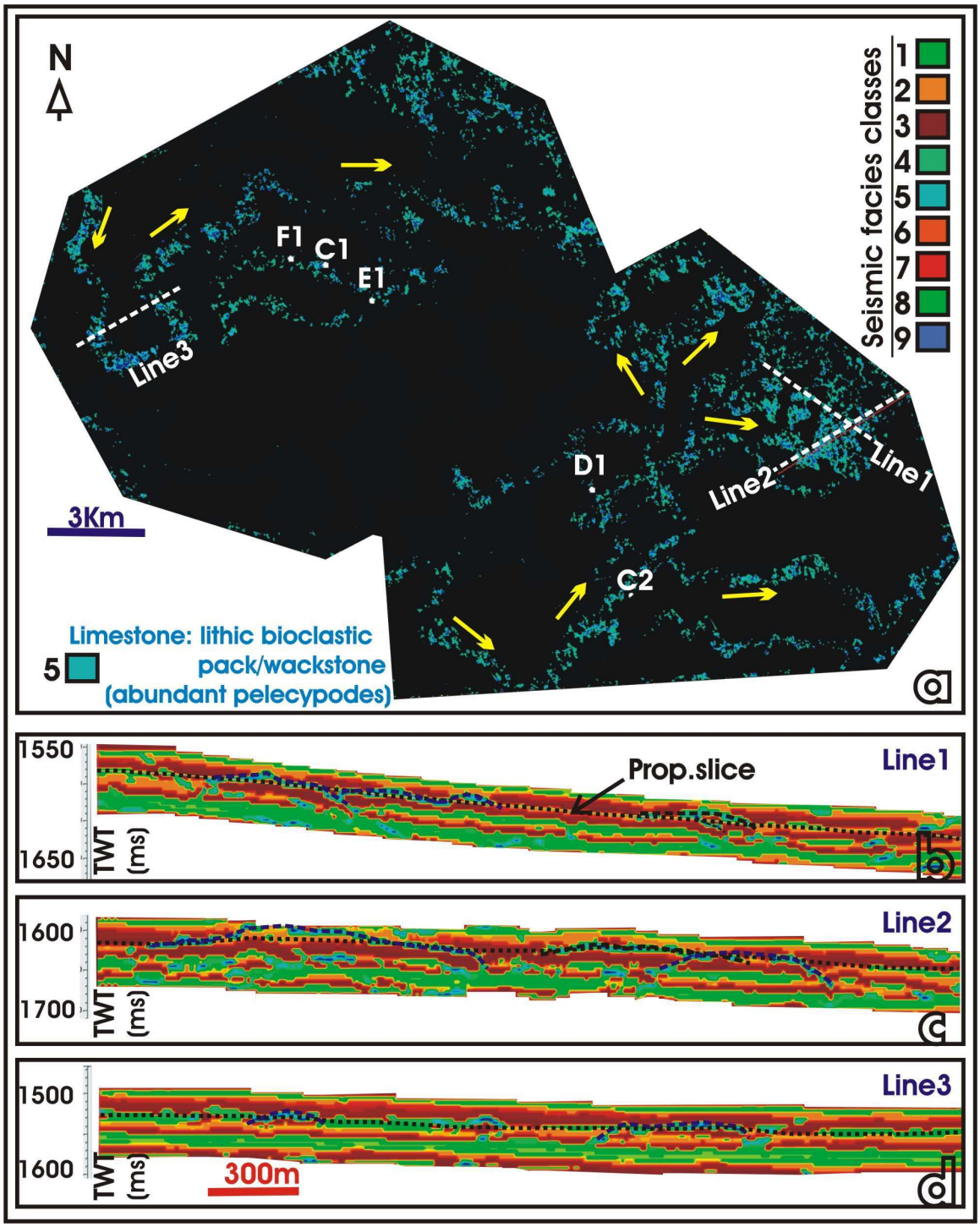
N
Seismic facies classes
1
2
3
4
5
6
7
8
9
F1
C1
E1
Line3
D1
Line2
Line1
C2
3Km
Limestone: lithic bioclastic
pack/wackstone
(abundant pelecypodes)
5
a
1550
1650
TWT (ms)
Prop.slice
Line1
b
1600
1700
TWT (ms)
Line2
c
1500
1600
TWT (ms)
300m
Line3
d

Figure 12